

Journal Pre-proofs

Research paper

Zn(II) and Cd(II) monomer, dimer and polymer compounds coordinated by benzoic acid and 4-acetylpyridine: Synthesis and crystal structures

Laura Moreno-Gómez, Francisco Sánchez-Férez, Teresa Calvet, Mercè Font-Bardia, Josefina Pons

PII: S0020-1693(20)30101-8
DOI: <https://doi.org/10.1016/j.ica.2020.119561>
Reference: ICA 119561

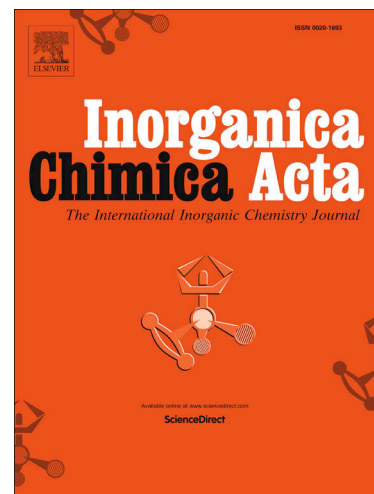
To appear in: *Inorganica Chimica Acta*

Received Date: 16 January 2020
Revised Date: 26 February 2020
Accepted Date: 28 February 2020

Please cite this article as: L. Moreno-Gómez, F. Sánchez-Férez, T. Calvet, M. Font-Bardia, J. Pons, Zn(II) and Cd(II) monomer, dimer and polymer compounds coordinated by benzoic acid and 4-acetylpyridine: Synthesis and crystal structures, *Inorganica Chimica Acta* (2020), doi: <https://doi.org/10.1016/j.ica.2020.119561>

This is a PDF file of an article that has undergone enhancements after acceptance, such as the addition of a cover page and metadata, and formatting for readability, but it is not yet the definitive version of record. This version will undergo additional copyediting, typesetting and review before it is published in its final form, but we are providing this version to give early visibility of the article. Please note that, during the production process, errors may be discovered which could affect the content, and all legal disclaimers that apply to the journal pertain.

© 2020 Published by Elsevier B.V.



**Zn(II) and Cd(II) monomer, dimer and polymer compounds
coordinated by benzoic acid and 4-acetylpyridine: Synthesis and
crystal structures**

Laura Moreno-Gómez,^a Francisco Sánchez-Férez,^a Teresa Calvet,^b Mercè Font-Bardia,^c
and Josefina Pons,^{a,*}

^aDepartament de Química, Universitat Autònoma de Barcelona, 08193-Bellaterra,
Barcelona, Spain

^bMineralogia, Petrologia i Geologia Aplicada, Universitat de Barcelona, Martí i
Franquès s/n, 08028-Barcelona, Spain.

^cUnitat de Difracció de Raig-X, Centres Científics i Tecnològics de la Universitat de
Barcelona (CCiTUB), Universitat de Barcelona, Solé i Sabarís, 1-3, 08028-Barcelona,
Spain.

Abstract

Reaction of MO (MO = Metal oxide, M = Zn(II) or Cd(II)) with benzoic acid (HBz) in H₂O/MeOH mixture as solvent yields two benzoate compounds: [Zn(μ -Bz)₂]_n (**1**) and [Cd(Bz)₂(H₂O)₃] (**2**). In addition, the reaction between M(MeCO₂)₂ (M = Zn(II) or Cd(II)) with HBz and 4-acetylpyridine (4-AcPy) in a 1:2:4 molar ratio and in MeOH solution, leads to the formation of [Zn(μ -Bz)₂(4-AcPy)]₂ (**3**) and [Cd(μ -Bz)₂(4-AcPy)₂]₂ (**4**). These four compounds have been fully characterized by analytical and spectroscopic techniques. Besides, their crystal structures have been elucidated revealing a 1D coordination polymer (**1**), a monomer (**2**), a paddle-wheel (**3**) and a dimer (**4**). In **1**, the Zn(II) ion is four-coordinated in a tetrahedral geometry while in **3** is penta-coordinated in a square-pyramidal geometry. By contrast, compounds **2** and **4** exhibit seven-coordinated Cd(II) ions in a pentagonal-bipyramidal geometry. In these set of compounds, the benzoate ligand presents different coordination modes such as bidentate bridged (μ_2 - η^1 : η^1) (**1** and **3**), chelate (μ_1 - η^2) (**2**) and both bridged and chelate (μ_2 - η^2 : η^1) (**4**). Besides, their extended structures have been analyzed. Finally, the UV-Vis and fluorescence spectra of all the compounds have been recorded as well as their quantum yields calculated.

Zn(II), Cd(II); benzoic acid; 4-acetylpyridine ligand; X-ray crystal structures; quantum yield

Introduction

During the last decades two new classes of metal-organic materials (MOMs), supramolecular coordination compounds (SCCs) and coordination polymers (CPs) have emerged in the field of coordination chemistry. They have attracted a huge interest not only for their structural versatility but also for their hierarchical assembly and their applications in many fields including catalysis [1], chemical separation [2] or sensing [3].

The arrangement of these compounds is mainly based on the geometry of the metal center and the nature of the ligands, which direct the formation of the primary structural motif. From there, the growth of the crystal structure could be driven through intermolecular interactions, such as hydrogen bonds or π - π stacking, into SCCs [4] or *via* coordination bonds resulting in CPs [5]. Remarkable is the effect of additional factors as metal:ligand ratio, counterions or solvent occluded molecules, in the final structural inception. The main characteristic of SCCs is the capability of outperforming CPs in their industrial applications due to the enhanced host-guest interactions and wet-processability [6].

Carboxylic acids have been widely used in coordination chemistry as multifunctional ligands due to their large variety of coordination modes, yielding mono-, di-, tri- polynuclear and polymeric coordination complexes [7]. Simple aromatic monocarboxylate anions are ubiquitous and versatile ligands in coordination chemistry. Therefore, benzoic acid has attracted notable interest because either allows the synthesis of SCCs or CPs [8] and even more important their synthesis in water as solvent, the greenest and most abundant of all solvents [9].

As aforementioned, the geometry of the metal atom is one of the structural determining forces in these systems. In particular, M(II) ions with d^{10} electronic

configuration confer a wide range of coordination numbers and geometries [10]. In addition, Zn(II) carboxylate complexes are relevant in biological systems [11], as $[\text{Zn}(\text{aspirinate})_2(\text{H}_2\text{O})_2]$ which presents anti-convulsing activity [12]. Besides, Cd(II) carboxylates are interesting for their photochemical and photocatalytic properties [13], as well as their structural versatility [14].

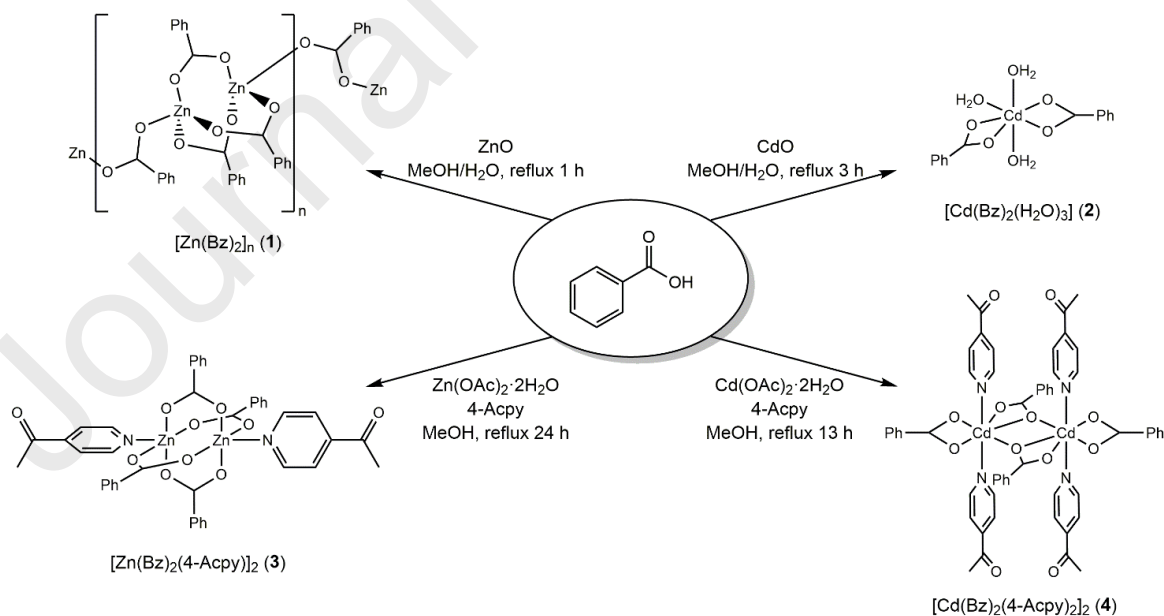
The synthesis of metal complexes by mixed ligand approach, combining carboxylate and heterocyclic *N*-donor ligands has enabled the obtainment of different physical, chemical and biological properties [15]. In addition, the reversible arrangement of the coordination bonds during the formation of the d^{10} metal complexes evolves into highly ordered structures [16].

Previously, our group have reported the preparation of Zn(II) and Cd(II) compounds either *via* direct reaction of carboxylic acids (1,3-benzodioxole-5-carboxylic (HPip); 3,5-dihydroxybenzoic (3,5-HDHB) or 3,5-dimethoxybenzoic (3,5-H(MeO)₂Bz)) or by mixed ligand strategy, combining these acids with different pyridine derivatives. The reaction of $\text{M}(\text{MeCO}_2)_2$ ($\text{M}=\text{Zn}(\text{II})$ or $\text{Cd}(\text{II})$) with HPip and 3- or 4-phenylpyridine resulted in two Zn(II) paddle-wheels and two Cd(II) dimers [17]. Unlike these previous results, the reaction between ZnO and 3,5-HDHB yielded a coordination polymer $[\text{Zn}(\mu\text{-3,5-DHB})_2(\text{H}_2\text{O})_2]_n$, which in presence of isonicotinamide (Isn), 4-acetylpyridine (4-Acpy) and 3-methylpyrazole (3-Mepz) generated monomeric complexes [18]. The role of 4,4'-bipyridine (4,4'-bpy) as linker *via* its reaction against $\text{Zn}(\text{MeCO}_2)_2$, 3,5-HDB or 3,5-H(MeO)₂Bz was also studied [19].

Recently, we have assayed the reaction between $\text{M}(\text{MeCO}_2)_2$ ($\text{M} = \text{Zn}(\text{II}), \text{Cd}(\text{II})$ or $\text{Hg}(\text{II})$) and HPip. While Zn(II) lead to a monomeric complex, Cd(II) and Hg(II) drove the formation of three coordination polymers with different nuclearity and

different coordination modes of the Pip ligand. In addition, their phosphorescence properties were recorded and their corresponding quantum yields calculated [20].

As a continuation of this study, in this paper we present the reaction of MO (M = Zn(II), Cd(II)) with HBz, which formed complexes $[\text{Zn}(\mu\text{-Bz})_2]_n$ (**1**) and $[\text{Cd}(\text{Bz})_2(\text{H}_2\text{O})_3]$ (**2**). Compound **1** is a coordination polymer while **2** presents a monomeric structure. Within this frame, the addition of 4-Acpy drove the formation of a paddle-wheel compound $[\text{Zn}(\mu\text{-Bz})_2(4\text{-Acpy})]_2$ (**3**) and a dimeric compound $[\text{Cd}(\mu\text{-Bz})_2(4\text{-Acpy})_2]_2$ (**4**). In these structures, the Bz ligand showed different coordination modes: chelate, bridged or both, and the incorporation of the 4-Acpy increased the coordination number, nuclearity and dimensionality of the resulting products (Scheme 1). Their molecular and supramolecular structures have been analyzed mainly associating *via* intermolecular hydrogen bond, π - π stacking and C-H \cdots O interactions. In addition, their UV-Vis and fluorescence spectra have been recorded and the corresponding quantum yields calculated.



Scheme 1. Outline of the synthesis of the complexes **1-4**.

Results and discussion

2.1. Synthesis and general characterization

Complexes **1** and **2** were obtained by direct reaction of benzoic acid (HBz) with ZnO or CdO, in a 1:2 molar ratio. Reactions were performed refluxing a solution of H₂O/methanol (35/10) mL for 1 h (**1**) or 24 h (**2**). Complexes **3** and **4** were obtained by mixing Zn(MeCO₂)₂·2H₂O or Cd(MeCO₂)₂·2H₂O with HBz and 4-Acpy ligands in a 1:2:4 molar ratio. These reactions were carried out for 3 h (**3**) or 13 h (**4**) in MeOH solution at reflux conditions.

Compounds **1-4** were characterized by powder X-Ray diffraction (PXRD), elemental analysis (EA), FTIR-ATR and ¹H NMR spectroscopies and single crystal X-ray diffraction method. In addition, their UV-Vis and phosphorescence spectra have been recorded and their quantum yields calculated. It should be noted that the structure of compound **1** was previously elucidated [8]. Nevertheless, we thought it appropriate to analyze and compare its supramolecular interactions, which were not previously studied.

Phase purity of the bulk samples was confirmed by PXRD. EA of all the compounds are in accordance with the proposed formula. FTIR-ATR spectra of compounds **1-4** display the characteristic bands of the Bz ligand. Besides, **3** and **4** also present bands attributable to the 4-Acpy ligand. The carboxylate bands of **1-4** appear between 1595 and 1501 cm⁻¹ for $\nu_{\text{as}}(\text{CO}_2)$ and between 1493 and 1391 cm⁻¹ for $\nu_{\text{s}}(\text{CO}_2)$ (SI: Figures S5-S8). For **1-4**, their Δ values ($\nu_{\text{as}}(\text{CO}_2) - \nu_{\text{s}}(\text{CO}_2)$) have been calculated: 170 (**1**), 110 (**2**), 176 (**3**), and 102, 156 (**4**) cm⁻¹. These values indicate a bidentate bridging coordination mode ($\mu_2\text{-}\eta^1\text{:}\eta^1$) of the carboxylate groups in **1** and **3** and a bidentate chelate coordination mode ($\mu_1\text{-}\eta^2$) in **2**. Finally, compound **4** presents two

values of Δ , inasmuch as the Bz ligand simultaneously has two coordination modes: bidentate bridged and chelate ($\mu_2\text{-}\eta^2\text{:}\eta^1$) [21].

Compound **2** also exhibits a broad band in the range 3419-3229 cm^{-1} , which corresponds to $\nu(\text{O-H})$ from water molecules coordinated to the Cd(II). For all the compounds, additional bands attributable to the aromatic groups $\nu(\text{C=C})/\nu(\text{C=N})$, $\delta(\text{C=C})/\delta(\text{C=N})$, $\delta(\text{C-H})_{\text{ip}}$ and $\delta(\text{C-H})_{\text{oop}}$ are also observed [22]. The FTIR-ATR spectral data thus, clearly lend support to the structures determined by the single crystal X-ray diffraction method.

^1H NMR spectra of the complexes **1-4** were recorded in DMSO- d_6 for **1**, D $_2$ O for **2**, and CDCl_3 for **3** and **4**, due to their different solubility. All the spectra show the signals belonging from Bz (**1, 2**) or Bz and 4-Acpy (**3, 4**) (SI: Figures S9-S12). The ^1H NMR spectra of all the compounds present three signals between 8.16 and 7.31 ppm assigned to the aromatic protons of the Bz ligand while those of the 4-Acpy appear at 8.89 ppm and 7.79 ppm (**3**) and at 8.90 ppm and 7.69 ppm (**4**). Moreover, the 4-Acpy present two signals at 2.65 (**3**) and 2.57 (**4**) ppm assigned to the CH_3 group [22]. The chemical shifts of *ortho*-benzoate and *ortho*-pyridyl groups are consistent with the presence of O_2C -coordinated and N -coordinated benzoate and pyridyl linkers, respectively.

2.2. Crystal and extended structure of compound **1**

The crystal structure of compound **1** was previously reported [8]. Although the syntheses were performed starting from $\text{Zn}(\text{CO}_3)$ [8.a] or ZnCl_2 [8.d] in this work has been performed with ZnO. Three of them ([8.a, 8.b and 8.d]) were elucidated at a different temperature (in this paper at 100K while the reported structures around 295K) exhibiting variation in the intermolecular interactions (*vide infra*) as previously reported in our group [23]. The last structure [8.c] was not studied and presented as a CSD

communication. The intermolecular interactions of these complexes were not studied and thus, the determination of the crystal structure allows the better comparison of the intermolecular interactions that hold together these structures.

Compound **1** has a polymeric *zig-zag* chain structure with a $[\text{ZnO}_4]$ core composed by four benzoate ligands in a bridging (*syn-syn* and *syn-anti*) coordination mode (Figure 1). The Zn(II) ions exhibit a slightly distorted tetrahedral geometry, $\tau_4 = 0.86$ (Zn(1)) and 0.94 (Zn(2)) [24], with angles ranging from $98.58(10)^\circ$ to $121.87(10)^\circ$ (Table 1).

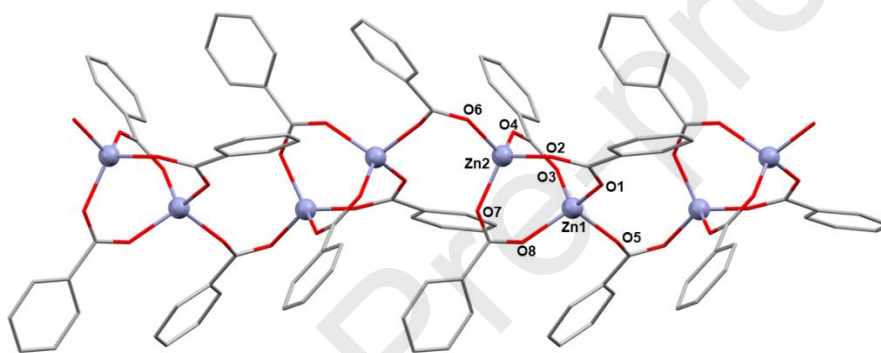


Figure 1. Molecular structure representation of compound **1**. Hydrogen atoms are omitted for clarity.

Compared to the reported structures [8], those determined at 295K [8.b] and 296K [8.d], present differences in the values of the Zn-O lengths and O-Zn-O angles (Zn(2)-O(2)#2, 1.954(2) and O(3)-Zn(1)-O(8)#1, 103.09(10) (present work); Zn(2)-O(8), 1.9792 and O(7)-Zn(1)-O(5) 112.26 [8.b]; Zn(1)-O(8)#1, 1.954(2) (present work); Zn(1)-O(8), 1.917(2) [8.d]). In compound **1**, the intermolecular interactions expand the structure forming 2D layers parallel to the *bc* plane (Figure 2a). This association is determined by weak C-H \cdots π interactions [25, 26] (C(20) \cdots Cg(1), 4.251 Å (work); C(4) \cdots Cg(1), 5.044 Å [8.b]; C(25) \cdots Cg(1), 5.026 Å [8.d]) between the *meta*-protons of the *syn-anti* Bz linkers and the *syn-syn* aromatic benzoate rings with the concomitant torsion of the *syn-anti* Bz rings (Table 1) (Figure 2b).

Table 1. Selected bond lengths (Å), bond angles (°) and intermolecular interactions for **1**.

Bond length (Å)				
Zn(1)-O(5)	1.938(2)	Zn(2)-O(6)	1.939(2)	
Zn(1)-O(3)	1.938(2)	Zn(2)-O(7)	1.940(2)	
Zn(1)-O(1)	1.938(2)	Zn(2)-O(4)#2	1.949(2)	
Zn(1)-O(8)#1	1.954(2)	Zn(2)-O(2)#2	1.954(2)	
Bond angles (°)				
O(5)-Zn(1)-O(3)	105.99(10)	O(6)-Zn(2)-O(7)	108.34(10)	
O(5)-Zn(1)-O(1)	98.66(9)	O(6)-Zn(2)-O(4)#2	111.96(10)	
O(3)-Zn(1)-O(1)	116.59(10)	O(7)-Zn(2)-O(4)#2	113.99(10)	
O(5)-Zn(1)-O(8)#1	109.62(10)	O(6)-Zn(2)-O(2)#2	98.58(10)	
O(3)-Zn(1)-O(8)#1	103.09(10)	O(7)-Zn(2)-O(2)#2	109.68(11)	
O(1)-Zn(1)-O(8)#1	121.87(10)	O(4)#2-Zn(2)-O(2)#2	113.17(10)	
Intermolecular interactions				
<i>D-H...A</i>	<i>D-H</i> (Å)	<i>H...A</i> (Å)	<i>D...A</i> (Å)	<i>> D-H...A</i> (°)
C(20)-H(20)...Cg(1)	0.950	3.481	4.251	139.88
#1 -x+1,y-1/2,-z+1/2 #2 -x+1,y+1/2,-z+1/2				
Cg1 (C(23) C(24) C(25) C(26) C(27) C(28))				

Although the structure elucidated at 100K [8.c] has a similar bond length and angles, the intermolecular C-H... π interaction also differs from our structure (C(20)-H(20)...Cg(1), 3.481 Å, C(20)...Cg(1), 4.251, 139.88° (present work); C(25)-H(25)...Cg(1), 4.712 Å, C(25)...Cg(1), 5.017 Å, 103.30° [8.c]).

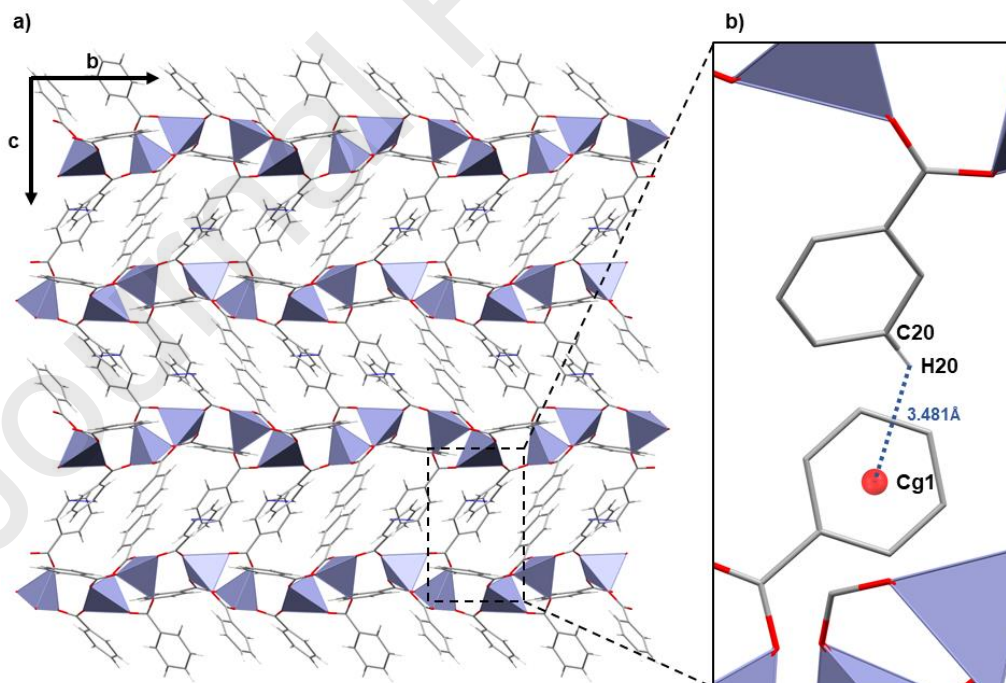


Figure 2. (a) Perpendicular view of the 2D layer generated by **1** along the *bc* plane. (b) *c* axis expansion via C-H... π interaction.

2.3. Crystal and extended structure of compound 2

Compound **2** belongs to the orthorhombic $Pbca$ space group. It has a monomeric structure with a $[CdO_7]$ core composed by two bidentate chelate benzoate ligands and three water molecules (Figure 3a). The Cd(II) ion exhibits a slightly distorted pentagonal-bipyramidal geometry [27] (Figures 3b and 3c) in which the equatorial plane is set by two Bz ligands and one H_2O molecule (ranging from $54.10(7)$ to $90.75(7)^\circ$) while the remaining two H_2O molecules hold the axial positions. Bond lengths and angles are provided in Table 2.

The pentagonal-bipyramidal is the most common geometry of hepta-coordinated metals, which in turn are less common than six- or eight-coordinated. This fact is due to a less effective packing arrangement caused by electronic repulsion and steric effects between ligands [28].

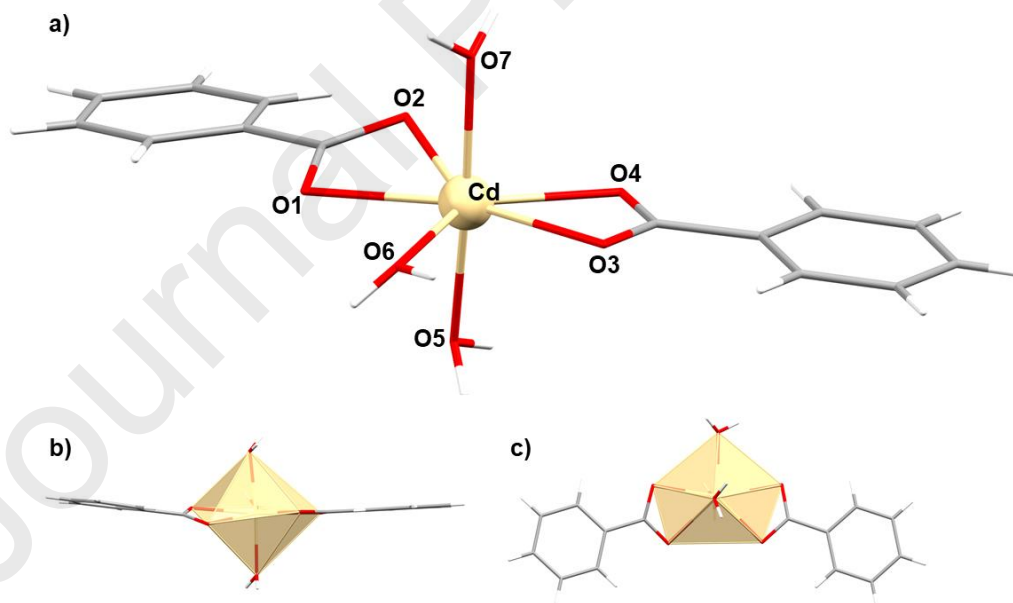


Figure 3. (a) Molecular structure representation of compound **2**. Front (b) and upper (c) view of the Cd(II) centers geometry.

In this case, the asymmetric chelated benzoate ligands enable this hepta-coordination. Similar Cd(II) polymeric compounds reported in the literature showed Cd-

O bond lengths and angles ranging between 2.277(6) and 2.487(5) Å and between 53.7(2) and 176.1(2)°, respectively [29].

In compound **2**, the supramolecular expansion is promoted by hydrogen bond interactions between the coordinated water molecules and the carboxylate oxygen atoms of the Bz ligands (Figure 4a) [30]. The equatorial water molecules exhibit hydrogen bond interactions along the *b* axis by only one proton (Figure 4b) while the axial water molecules present hydrogen bond interactions along the *ab* plane *via* both hydrogen atoms (Figures 4c).

All these set of interactions hold together the monomeric units forming 2D layers parallel to the *ab* plane. Bond lengths and angles related to hydrogen bond interactions are listed in Table 2.

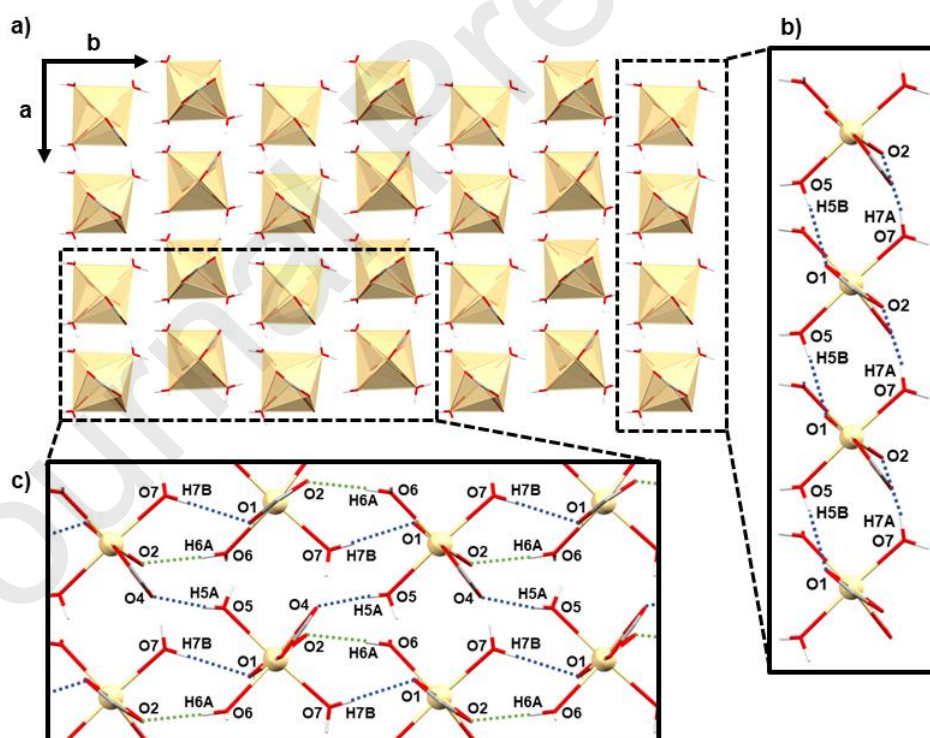


Figure 4. (a) Perpendicular view of the 2D layer generated by **2** along the *ab* plane. (b) Perpendicular view of the *a* axis and (c) *b* axis expansion *via* hydrogen bond interactions (highlighted in blue and green) through the axial and equatorial water molecules, respectively.

Table 2. Selected bond lengths (Å), bond angles (°) and intermolecular interactions for **2**.

Bond length (Å)				
Cd-O(1)	2.3741(19)	Cd-O(5)	2.277(2)	
Cd-O(2)	2.4670(19)	Cd-O(6)	2.323(2)	
Cd-O(3)	2.383(2)	Cd-O(7)	2.257(2)	
Cd-O(4)	2.334(2)			
Bond angles (°)				
O(7)-Cd-O(5)	173.38(8)	O(5)-Cd-O(3)	96.46(8)	
O(7)-Cd-O(6)	91.90(8)	O(6)-Cd-O(3)	79.03(7)	
O(5)-Cd-O(6)	92.52(8)	O(4)-Cd-O(3)	55.94(7)	
O(7)-Cd-O(4)	93.34(8)	O(1)-Cd-O(3)	160.36(7)	
O(5)-Cd-O(4)	87.06(8)	O(7)-Cd-O(2)	83.73(8)	
O(6)-Cd-O(4)	134.52(7)	O(5)-Cd-O(2)	89.65(7)	
O(7)-Cd-O(1)	94.69(8)	O(6)-Cd-O(2)	134.73(7)	
O(5)-Cd-O(1)	81.08(7)	O(4)-Cd-O(2)	90.75(7)	
O(6)-Cd-O(1)	81.61(7)	O(1)-Cd-O(2)	54.10(7)	
O(4)-Cd-O(1)	142.61(7)	O(3)-Cd-O(2)	145.53(7)	
O(7)-Cd-O(3)	89.22(8)			
Intermolecular interactions				
<i>D-H...A</i>	<i>D-H</i> (Å)	<i>H...A</i> (Å)	<i>D...A</i> (Å)	> <i>D-H...A</i> (°)
O(5)-H(5B)···O(1)	0.766(5)	2.018(5)	2.777(3)	170.77(4)
O(7)-H(7A)···O(2)	0.800(2)	1.973(2)	2.748(3)	162.92(3)
O(5)-H(5A)···O(4)	0.833(4)	1.848(4)	2.658(3)	163.69(4)
O(7)-H(7B)···O(1)	0.799(2)	1.990(2)	2.783(3)	171.45(3)
O(6)-H(6A)···O(2)	0.801(2)	1.996(2)	2.797(3)	177.92(3)

2.4. Crystal and extended structure of compound **3**

Compound **3** belongs to the monoclinic C2/c space group. There are two crystallographically independent dimeric units with similar bond lengths and angles present in the unit cell (Molecule A and B) (Figure 5).

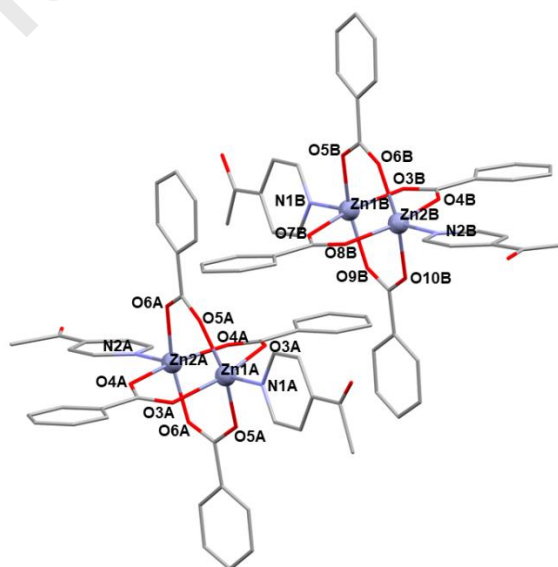


Figure 5. Molecular structure representation of compound **3** showing the two crystallographically independent units comprised in the unit cell (A left, B right). Hydrogen atoms are omitted for clarity.

Both display a dimeric paddle-wheel like structure with a $[\text{ZnO}_4\text{N}]$ core. The dimeric units are composed by four bidentate bridging benzoate ligands in a *syn-syn* disposition, which join the two Zn(II) centers and two monodentate 4-Acpy ligands. These Zn(II) ions exhibit a slightly distorted square-pyramidal geometry ($\tau = 0.01\text{-}0.06$) [31] with an elongation (0.355-0.398 Å) from the basal plane towards the axial position.

Table 3. Selected bond lengths (Å), bond angles (°) and intermolecular interactions for **3**.

Molecule A				
<i>Bond length (Å)</i>				
Zn(1A)-O(5A)	2.015(2)	Zn(2A)-N(2A)	2.015(4)	
Zn(1A)-N(1A)	2.032(4)	Zn(2A)-O(6A)	2.037(3)	
Zn(1A)-O(3A)	2.046(2)	Zn(2A)-O(4A)	2.046(3)	
<i>Bond angles (°)</i>				
O(5A)-Zn(1A)-O(5A)#1	155.81(15)	O(6A)#1-Zn(2A)-O(6A)	161.53(15)	
O(5A)-Zn(1A)-N(1A)	102.10(8)	N(2A)-Zn(2A)-O(4A)#1	101.04(8)	
O(5A)-Zn(1A)-O(3A)#1	87.87(11)	O(6A)-Zn(2A)-O(4A)#1	88.36(11)	
O(5A)-Zn(1A)-O(3A)	87.74(11)	N(2A)-Zn(2A)-O(4A)	101.04(8)	
N(1A)-Zn(1A)-O(3A)	100.52(7)	O(6A)-Zn(2A)-O(4A)	88.12(11)	
O(3A)#1-Zn(1A)-O(3A)	158.95(15)	O(4A)#1-Zn(2A)-O(4A)	157.92(16)	
N(2A)-Zn(2A)-O(6A)	99.23(8)	O(6A)#1-Zn(2A)-O(6A)	161.53(15)	
Molecule B				
<i>Bond length (Å)</i>				
Zn(1B)-O(9B)	2.005(3)	Zn(2B)-O(4B)	2.012(3)	
Zn(1B)-N(1B)	2.012(3)	Zn(2B)-N(2B)	2.027(3)	
Zn(1B)-O(5B)	2.041(3)	Zn(2B)-O(8B)	2.031(3)	
Zn(1B)-O(7B)	2.052(3)	Zn(2B)-O(10B)	2.067(3)	
Zn(1B)-O(3B)	2.054(3)	Zn(2B)-O(6B)	2.080(3)	
<i>Bond angles (°)</i>				
O(9B)-Zn(1B)-N(1B)	98.25(13)	O(4B)-Zn(2B)-N(2B)	98.95(12)	
O(9B)-Zn(1B)-O(5B)	160.04(14)	O(4B)-Zn(2B)-O(8B)	161.29(12)	
N(1B)-Zn(1B)-O(5B)	101.60(13)	N(2B)-Zn(2B)-O(8B)	99.74(12)	
O(9B)-Zn(1B)-O(7B)	86.68(14)	O(4B)-Zn(2B)-O(10B)	87.07(12)	
N(1B)-Zn(1B)-O(7B)	99.05(12)	N(2B)-Zn(2B)-O(10B)	100.35(12)	
O(5B)-Zn(1B)-O(7B)	88.19(15)	O(8B)-Zn(2B)-O(10B)	90.38(13)	
O(9B)-Zn(1B)-O(3B)	89.48(13)	O(4B)-Zn(2B)-O(6B)	87.62(11)	
N(1B)-Zn(1B)-O(3B)	101.81(12)	N(2B)-Zn(2B)-O(6B)	100.82(12)	
O(5B)-Zn(1B)-O(3B)	88.47(14)	O(8B)-Zn(2B)-O(6B)	88.08(12)	
O(7B)-Zn(1B)-O(3B)	159.12(13)	O(10B)-Zn(2B)-O(6B)	158.73(13)	
Intermolecular interactions				
<i>D-H...A</i>	<i>D-H (Å)</i>	<i>H...A (Å)</i>	<i>D...A (Å)</i>	<i>> D-H...A (°)</i>
Cg(1)...Cg(2)			3.669	
Cg(3)...Cg(4)			3.689	
C(40)-H(40)...Cg(5)	0.950	2.777	3.698	163.33
C(32)-H(32)...O(2)	0.950	2.777	3.547(5)	138.80

#1 -x+2,y,-z+3/2

The basal plane is formed by four oxygen atoms from the Bz ligands with bond angles between 86.68(14)-90.38(13)° (Table 3), while the 4-Acpy ligand holds the

apical position. Other reported Zn(II) paddle-wheel benzoates containing different heterocyclic nitrogen donors showed similar bond lengths (2.018-2.083 Å) and bond angles (between 86.47-159.36°): [Zn₂(py)₂(Bz)₄] (py = pyridine) [32] and [Zn₂(Bz)₄(2,5-Me₂pyz)]_n (2,5-Me₂pyz = 2,5-dimethylpyrazine) [11].

The paddle-wheel units in **3** are hold together *via* weak π - π , C-H \cdots π and C-H \cdots O interactions. Bz ligands stack with the 4-Acpy ligands by π - π interactions at 3.669 Å (Cg1-Cg2). In addition, they also drive π - π (3.689 Å, Cg3-Cg4) and a C-H \cdots π (3.698 Å) interactions with other Bz ligands from neighboring paddle-wheels through their H_{para} protons (Table 3). Finally, Bz ligand also promotes weak C-H \cdots O interactions between the H_{meta} and the carbonyl group of the 4-Acpy (2.777 Å). Planar π - π interactions expands along the *c* axis while C-H \cdots π and C-H \cdots O interactions expands it along *a* and *b* axis, respectively, forming a 3D supramolecular structure (Figure 6).

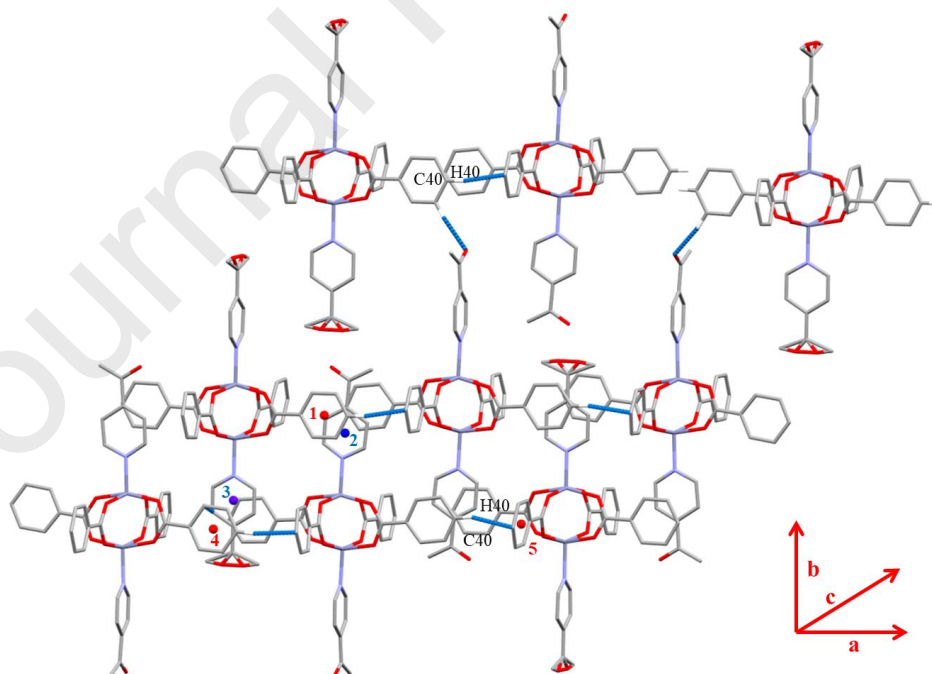


Figure 6. Supramolecular expansion of compound **3**. Blue (4-Acpy) and red (Bz) centroids implied in the intermolecular interactions are highlighted.

2.5. Crystal and extended structure of compound **4**

Compound **4** belongs to the tetragonal $P4_12_12$ space group. It has a dimeric structure with four benzoate ligands and four 4-Acpy ligands. Each cadmium atom adopts a $[CdO_5N_2]$ core (Figure 7a). The dimeric unit is composed by two bidentate benzoate ligands exhibiting both chelate and bridged coordination modes. One of the carboxylate oxygen atoms is bonded to the Cd(II) center while the other acts as ditopic linker joining both Cd(II) ions.

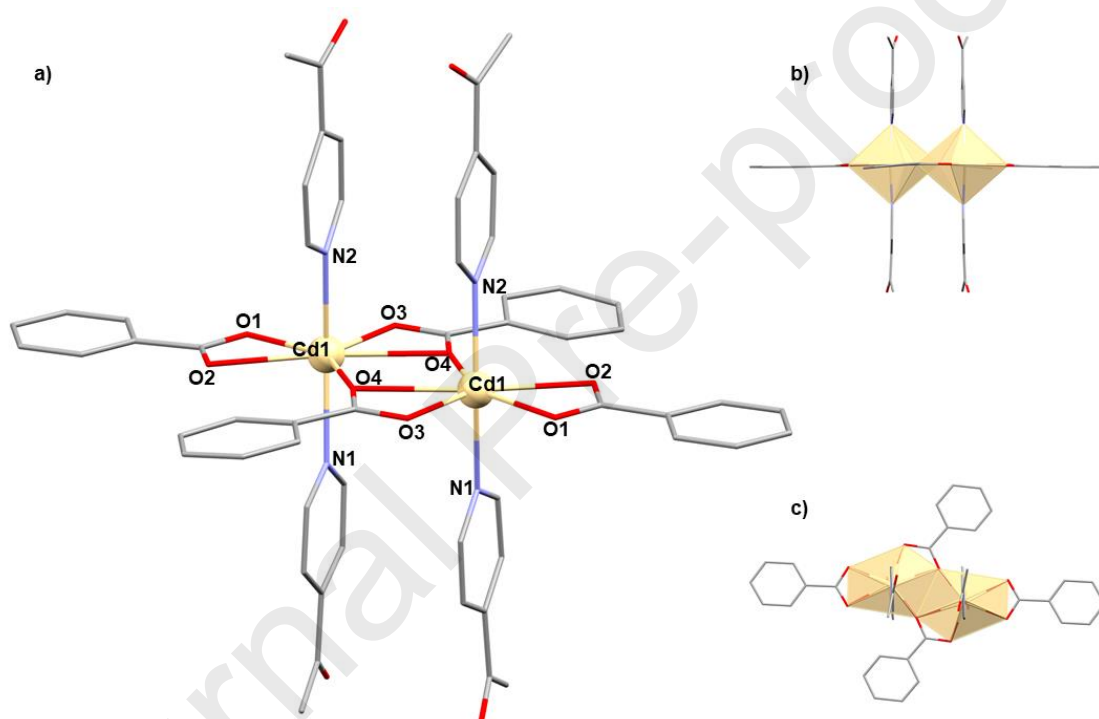


Figure 7. (a) Molecular structure representation of compound **4**. Front (b) and upper (c) view of the Cd(II) centers geometry.

These metal centers exhibit a slightly distorted pentagonal-bipyramidal geometry [27] and all the benzoate ligands are arranged in the equatorial plane, with equatorial angles between $52.98(7)$ - $92.87(7)^\circ$ (Table 4). The four 4-Acpy ligands hold the axial positions (Figures 7b and 7c). There are similar Cd(II) compounds with comparable bond lengths ($2.314(4)$ - $2.520(5)$ Å) and bond angles (52.98 to 173.74°) [27].

These dimeric units are held together forming a 3D net *via* weak C-H \cdots O and C-H \cdots π interactions (Figure 8). Lengths and angles related to these interactions are shown in Table 4.

Table 4. Selected bond lengths (Å), bond angles (°) and intermolecular interactions for **4**.

Bond length (Å)				
Cd(1)-O(1)	2.291(2)	Cd(1)-O(4)#1	2.344(2)	
Cd(1)-O(3)	2.315(2)	Cd(1)-O(2)	2.5149(19)	
Cd(1)-N(2)	2.331(3)	Cd(1)-O(4)	2.577(2)	
Cd(1)-N(1)	2.338(3)			
Bond angles (°)				
O(1)-Cd(1)-O(3)	84.89(8)	O(3)-Cd(1)-O(2)	139.22(7)	
O(1)-Cd(1)-N(2)	95.47(11)	N(2)-Cd(1)-O(2)	90.01(9)	
O(3)-Cd(1)-N(2)	93.65(10)	N(1)-Cd(1)-O(2)	87.51(9)	
O(1)-Cd(1)-N(1)	92.58(11)	O(4)#1-Cd(1)-O(2)	92.87(7)	
O(3)-Cd(1)-N(1)	95.87(10)	O(1)-Cd(1)-O(4)	137.85(7)	
N(2)-Cd(1)-N(1)	168.04(9)	O(3)-Cd(1)-O(4)	52.98(7)	
O(1)-Cd(1)-O(4)#1	147.17(7)	N(2)-Cd(1)-O(4)	89.33(9)	
O(3)-Cd(1)-O(4)#1	127.91(7)	N(1)-Cd(1)-O(4)	90.63(9)	
N(2)-Cd(1)-O(4)#1	84.81(9)	O(4)#1-Cd(1)-O(4)	74.93(7)	
N(1)-Cd(1)-O(4)#1	83.63(9)	O(2)-Cd(1)-O(4)	167.79(6)	
O(1)-Cd(1)-O(2)	54.34(7)			
Intermolecular interactions				
<i>D-H\cdotsA</i>	<i>D-H</i> (Å)	<i>H\cdotsA</i> (Å)	<i>D\cdotsA</i> (Å)	<i>> D-H\cdotsA</i> (°)
C(13)-H(13) \cdots O(3)	0.950	2.541	3.338(4)	141.56
C(7)-H(7) \cdots Cg(1)	0.950	3.514	3.974	112.35
C(16)-H(16) \cdots Cg(2)	0.950	3.479	4.231	137.77
C(25)-H(25) \cdots Cg(2)	0.950	2.925	3.794	152.76

#1 y,x,-z+1

Cg1 (C(9) C(10) C(11) C(12) C(13) C(14)); Cg2 (C(2) C(3) C(4) C(5) C(6) C(7))

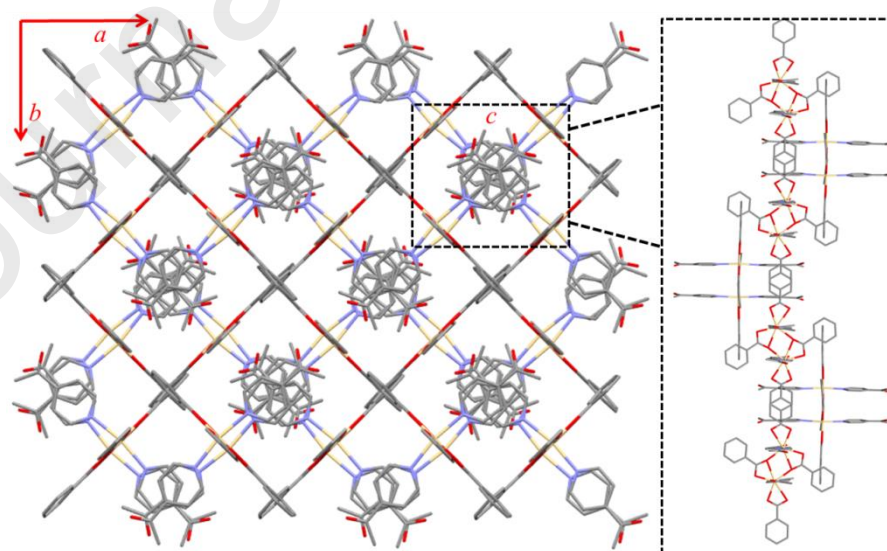


Figure 8. Perpendicular view of the *ab* expansion of compound **4** (left). In detail of *c* axis expansion (right).

2.6. UV-Vis and photoluminescence experiments

The UV-Vis and fluorescence spectra of complexes **1**, **3** and **4** have been performed in MeOH solution while the spectra of **2** in H₂O. All the experiments have been recorded between 190 and 320 nm at 298 K. The UV-Vis measurements of L-tyrosine, HBz and 4-Acapy ligands, and complexes **1-4**, have been carried out with a concentration ranging from $1 \cdot 10^{-9}$ to $1 \cdot 10^{-4}$ M to ensure their no aggregation (S.I.: Fig. S13-S14).

L-tyrosine used as reference also displayed three λ_{\max} at 193, 222 and 275 nm. The HBz as well as the 4-Acapy ligand presents three absorption peaks (λ_{\max}) at 202, 224, 271 nm and 203, 220, 278 nm, respectively. Compounds **1-4** present λ_{\max} bands centered around 200, 222 and 270 nm. Considering the conjugation of the aromatic rings present in both ligands as well as the lone pairs of the nitrogen and oxygen atoms, there are several potential transitions in these complexes, rising from $\pi-\pi^*$, $n-\pi^*$ and $n-\sigma^*$ [33]. The absorbance of the complexes at 270 nm increase $2 < 3 < 1 < 4$, in that order (Figure 9).

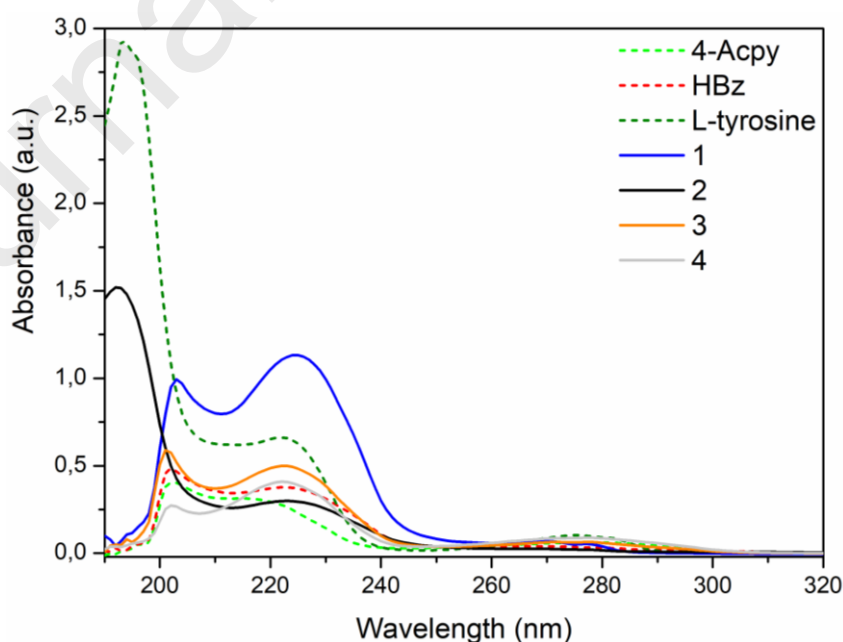


Figure 9. UV-Vis absorption spectra of L-tyrosine, 4-Acapy and HBz ligands and complexes **1-4** recorded between 190 and 320 nm.

The emission spectra of L-tyrosine, HBz and 4-Acpy ligands and complexes **1-4**, have been measured at 298 K. All the experiments have been performed with an λ_{exc} of 270 nm and recording between 280 and 470 nm. The concentrations used were $9.75 \cdot 10^{-6}$ M (L-tyrosine) for the standard, $1.68 \cdot 10^{-7}$ M (HBz) and $1.68 \cdot 10^{-7}$ M (4-Acpy) for the ligands, and $8.11 \cdot 10^{-8}$ M (**1**), $1.10 \cdot 10^{-7}$ M (**2**), $6.46 \cdot 10^{-8}$ M (**3**) and $4.16 \cdot 10^{-6}$ M (**4**) for the complexes. Their emission spectra have been depicted in Figure 10.

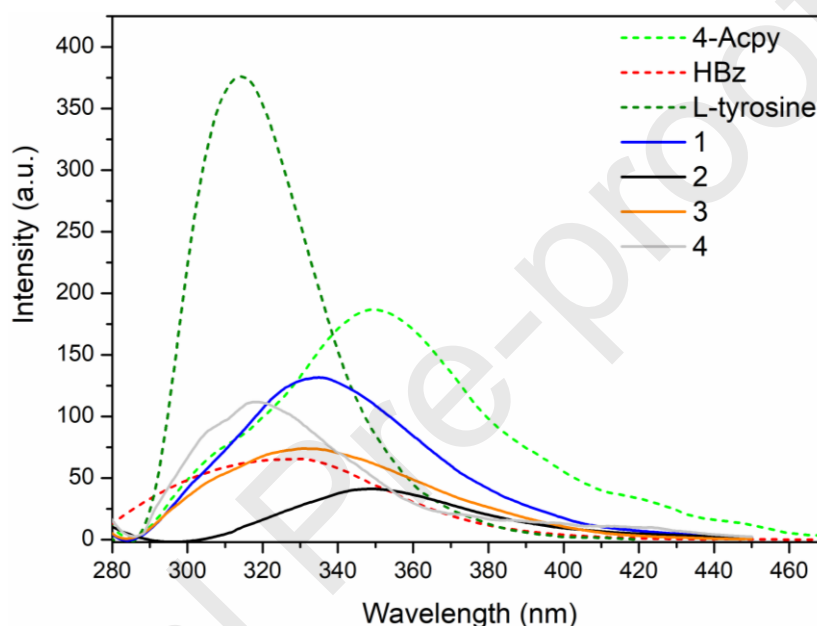


Figure 10. Emission spectra of L-tyrosine, 4-Acpy and HBz ligands and complexes **1-4** excited at 270 nm and recorded between 280 and 470 nm.

Fluorescence quantum yield (φ_s) is defined as the ratio of the number of photons emitted to the number of photons absorbed and describes how a fluorophore converts the excitation light into fluorescence [34]. The relative fluorescence quantum yield is calculated relating the quantum yield value of the desired compound and comparing with a reference (standard) [35].

The quantum yields of compounds **1-4** have been calculated using equation 1,

$$\varphi_s = \varphi_r \left(\frac{OD_{ref}}{OD_s} \right) \left(\frac{I_s}{I_{ref}} \right) \left(\frac{n_s}{n_{ref}} \right)^2 \quad (\text{eq. 1})$$

where φ_{ref} and φ_s , are the quantum yields of the reference and the sample, respectively. I is the area under the curve for the emission spectra, OD is the optical density (or absorbance), and n is the refractive index of the solvent. L-tyrosine has been used as a standard ($\varphi_{ref} = 0.14$) [36]. The values of A_{ref} and I_{ref} for L-tyrosine as well as for compound **2** have been recorded using Milli-Q water as solvent ($n_{ref} = 1.3325$) [37]. The values of A_s and I_s of HBz and 4-AcPy ligands and compounds **1**, **3** and **4** have been measured using MeOH as solvent ($n_s = 1.3314$) [37] at r.t. The values of relative quantum yields obtained for compounds **1-4** are 0.034 (**1**), 0.012 (**2**), 0.021 (**3**) and 0.026 (**4**) (Table 5).

Table 5. Fluorescence data for quantum yield calculations (φ_s).

Sample	λ_{abs} (nm)	λ_{em} (nm)	Solvent	Refractive index [36]	Absorbance (a.u.)	Area	Quantum yield
L-tyrosine	193, 222, 275	314	Water	1.3325	0.030	21525.7	0.14 [37]
4-AcPy	203, 222, 278	350	MeOH	1.3314	0.054	14097.3	0.051
HBz	202, 224, 271	330	MeOH	1.3314	0.041	4602.45	0.022
1	203, 225, 270	334	MeOH	1.3314	0.049	8572.74	0.034
2	192, 223, 269	349	Water	1.3325	0.043	2622.32	0.012
3	201, 222, 272	332	MeOH	1.3314	0.048	5286.73	0.021
4	202, 222, 277	318	MeOH	1.3314	0.049	6545.58	0.026

The complexation of the HBz ligand to the metal center resulted in a bathochromic shift in **2** while compound **4** shows a hyperchromic shift respect to both HBz and 4-AcPy ligands. Photoluminescence in **1** is probably favored by the increased rigidity of the ligand in the polymeric array, with concomitant decrease of radiation, the minor decay process of the intraligand ($\pi-\pi^*$) excited state and the reduced energy loss driven by the intramolecular or intermolecular interactions of the organic linker [39]. Compared to **1**, the incorporation of the 4-AcPy ligand caused a decay in the emission probably driven by the less structural rigidity of the dimeric array (**3**). In presence of HBz ligand, the Cd(II) center formed a monomeric array (**2**) which could easily transfer the absorbed energy to other relaxation processes. Finally, as opposed to the Zn(II)

complexes, the addition of the 4-Acpy to the Cd(II) center resulted in a more rigid structure and its consequent increase in quantum yield.

Conclusions

In this paper, we present the reactivity of HBz against MO or $M(\text{MeCO}_2)_2$ and 4-Acpy ($M = \text{Zn(II)}$ or Cd(II)). The study of their coordination has revealed the formation of compounds with different nuclearity and dimensionality, from monomers to polymers (**1-4**). These compounds presented a great variety of coordination numbers: four (**1**), five (**3**) and seven (**2** and **4**), and different coordination modes of the carboxylate groups (bidentate chelate, bridged or both). Their coordination numbers increase with the size of metal (**1** and **2**) or (**3** and **4**) and also increase with the presence of the 4-Acpy (**1** and **3**) or (**2** and **4**). The higher coordination number in **2** and **4** is reasonably understood by the large ionic radius of the Cd(II) centers. Although in **2** the water coordination facilitated the increase of coordination number, it should be noted that in the case of compound **4**, the chelate and bridging coordination mode of the Bz ligands enable this seven-coordination. Thus, the structural differences of complexes **1-4** are determined by both the metal size and the incorporation of the 4-Acpy ligand.

The structural analysis evinced that complexes **1** and **2** form 2D layers while **3** and **4** form 3D network supported by hydrogen bonds (**2**) and weak interactions: $\text{C-H}\cdots\pi$ (**1**, **2**, **4**), π - π and $\text{C-H}\cdots\text{O}$ (**3**, **4**). In addition, the luminescence properties of all the complexes and the ligands have been analyzed and their quantum yields calculated (**1**>**4** >**3**>**2**).

Experimental Section

4.1 Materials and general details

Zinc(II) oxide nanopowder (ZnO), cadmium(II) oxide (CdO), zinc(II) acetate dihydrate ($\text{Zn}(\text{OAc})_2 \cdot 2\text{H}_2\text{O}$), cadmium(II) acetate dihydrate ($\text{Cd}(\text{OAc})_2 \cdot 2\text{H}_2\text{O}$), benzoic acid (HBz), 4-acetylpyridine (4-Acpy) and methanol (MeOH) were purchased from Sigma-Aldrich and deuterated dimethyl sulfoxide ($\text{DMSO-}d_6$), deuterated chloroform (CDCl_3) and deuterated water (D_2O) were purchased from Eurisotop. All products were used without further purification. All the reactions were carried out at reflux conditions, in MeOH for compounds **1** and **3** and in MeOH/ H_2O for compounds **2** and **4**. Powder X-ray diffraction (PXRD) patterns were measured with Siemens D5000 apparatus (with 40 kW and 45 mA using $\text{CuK}\alpha$ radiation with $\lambda = 1.5406 \text{ \AA}$). All of them were recorded from $2\theta = 5^\circ$ to 30° with a step scan of 0.02° counting 1s at each step. Elemental analyses (C, H, N) were carried out on a Thermo Scientific Flash 2000 CHNS Analyzer. FTIR-ATR spectra were recorded on a Tensor 27 (Bruker) spectrometer, equipped with an attenuated total reflectance (ATR) accessory model MKII Golden Gate with diamond window in the range $4000\text{-}500 \text{ cm}^{-1}$. ^1H NMR spectra were recorded on an NMR-FT Bruker 360 MHz and 400 MHz spectrometers in $\text{DMSO-}d_6$ solution for compound **1**, in D_2O solution for compound **3** and in CDCl_3 solution for compounds **2** and **4**. All chemical shifts (δ) are given in ppm relative to TMS as internal standard. The electronic spectra in MeOH (**1**, **3** and **4**) or H_2O (**2**) solution (from $\sim 1 \cdot 10^{-9} \text{ M}$ to $\sim 1 \cdot 10^{-4} \text{ M}$) were run on a Agilent HP 8453 UV-Vis spectrophotometer with a quartz cell having path length of 1 cm in the range of 195-320 nm. Fluorescence measurements were carried out with a PerkinElmer LS 55 50 Hz fluorescence spectrometer using a 1cm quartz cell, in MeOH (**1**, **3** and **4**) or H_2O (**2**) solution. The samples were excited at 270 nm and the emission spectra were recorded between 285 and 450 nm at 297 K. The data obtained

were corrected for the dilution effects by means of the Origin Pro 8 software. FTIR-ATR and $^1\text{H-NMR}$ spectra were generated using Origin Pro 8.6 and MestReNova programs.

4.2 Synthesis of the compound $[\text{Zn}(\mu\text{-Bz})_2]_n$ (**1**)

A H_2O suspension (35 mL) of ZnO (151 mg, 1.86 mmol) was added dropwise to a MeOH solution (10 mL) of HBz (451 mg, 3.69 mmol) and stirred for 15 h at room temperature (r.t.). Then, the solution was stirred under reflux conditions for 1 h and a white powder precipitated. The resulting solid was filtered, washed with 10 mL cold MeOH and dried under vacuum. Mother liquors were concentrated until half of the volume and colorless crystals were obtained after 1 h.

Yield: 131 mg (23%). Anal. Calc. for $\text{C}_{28}\text{H}_{20}\text{O}_8\text{Zn}_2$ ($615.18 \text{ g mol}^{-1}$): C, 54.66; H, 3.28. Found: C, 54.54; H, 3.14%. ATR-FTIR (wavenumber, cm^{-1}): 3061(w), 3030(w) [$\nu(\text{CH})_{\text{ar}}$], 1575(m) [$\nu_{\text{as}}(\text{COO})$], 1551-1527(br) [$\nu(\text{C}=\text{C})$, $\nu(\text{C}=\text{N})_{\text{ar}}$], 1405(s) [$\nu_{\text{s}}(\text{COO})$], 1026(m) [$\delta_{\text{ip}}(\text{C-H})$], 712(s), 675(s) [$\delta_{\text{oop}}(\text{C-H})$]. $^1\text{H-NMR}$: (400 MHz, $\text{DMSO-}d_6$ solution, Me_4Si , 298 K) δ : 7.95 [2H, m, *ortho-H*_{Bz}], 7.49 [1H, tt, $^3J = 7.3 \text{ Hz}$, $^4J = 1.8 \text{ Hz}$, *para-H*_{Bz}], 7.41 [2H, m, *meta-H*_{Bz}] ppm. (UV-Vis: (MeOH , $8.11 \times 10^{-8} \text{ M}$) $\lambda_{\text{max}} = 203 \text{ nm}$; 225 nm; 270 nm.

4.3 Synthesis of the compound $[\text{Cd}(\text{Bz})_2(\text{H}_2\text{O})_3]$ (**2**)

A H_2O suspension (35 mL) of CdO (150 mg, 1.17 mmol) was added dropwise to a MeOH solution (10 mL) of HBz (286 mg, 2.34 mmol) and stirred for 2 h at r.t. Then, the solution was stirred under reflux conditions for 3 h. The resulting colorless solution was vacuumed until a white powder precipitated. The solid obtained was filtered and washed with 10 mL of cold MeOH . After six days, colorless crystals were obtained *via* recrystallization of compound **2** in H_2O solution.

Yield: 58.4 mg (57%). Anal. Calc. for $C_{14}H_{16}O_7Cd$ (408.67 gmol^{-1}): C, 41.14; H, 3.95. Found: C, 40.84; H, 3.91%. ATR-FTIR (wavenumber, cm^{-1}): 3419-3229(br) $[\nu(\text{OH})]_{\text{water}}$, 3087(w), 3054(w), 3030(w) $[\nu(\text{CH})]_{\text{ar}}$, 1501(m) $[\nu_{\text{as}}(\text{COO})]$, 1391(s) $[\nu_{\text{s}}(\text{COO})]$, 1024(m) $[\delta_{\text{ip}}(\text{C-H})]$, 712(s), 679(s) $[\delta_{\text{oop}}(\text{C-H})]$. $^1\text{H-NMR}$: (250 MHz, D_2O solution, Me_4Si , 298 K) δ : 7.87 [2H, br, *ortho-H*_{Bz}], 7.54 [1H, br, *para-H*_{Bz}], 7.47 [2H, br, *meta-H*_{Bz}] ppm. (UV-Vis: (H_2O , $1.1 \times 10^{-7} \text{ M}$) $\lambda_{\text{max}} = 192 \text{ nm}$; 223 nm; 269 nm.

4.4 Synthesis of the compound $[\text{Zn}(\mu\text{-Bz})_2(4\text{-Acpy})]_2$ (3)

A MeOH solution (10 mL) of HBz (111 mg, 0.911 mmol) with 4-Acpy (219 mg, 1.81 mmol) was added dropwise to a MeOH solution (6 mL) of $\text{Zn}(\text{OAc})_2 \cdot 2\text{H}_2\text{O}$ (99.7 mg, 0.454 mmol) and stirred for 2 days at r.t. Then, the solution was stirred under reflux conditions for 24 h. The resulting white suspension was cooled down and concentrated until half of the volume. Suitable crystals were grown from the mother liquors in 1 h. Crystals were filtered and washed with 10 mL of cold MeOH.

Yield: 366 mg (77%). Anal. Calc. for $C_{42}H_{34}N_2O_{10}Zn_2$ (857.45 gmol^{-1}): C, 58.43; H, 4.00; N, 3.27. Found: C, 58.72; H, 3.84; N, 3.05%. ATR-FTIR (wavenumber, cm^{-1}): 3055(w), 3008(w) $[\nu(\text{CH})]_{\text{ar}}$, 2920(w) $[\nu(\text{CH})]_{\text{al}}$, 1703(m) $[\nu(\text{C=O})]_{4\text{-Acpy}}$, 1574(m) $[\nu_{\text{as}}(\text{COO})]$, 1553(w) $[\nu(\text{C=C}), \nu(\text{C=N})]_{\text{ar}}$, 1398(s) $[\nu_{\text{s}}(\text{COO})]$, 1359(m) $[\delta(\text{C=C}), \delta(\text{C=N})]_{\text{ar}}$, 1024(w) $[\delta_{\text{ip}}(\text{C-H})]$, 718(s), 677(s) $[\delta_{\text{oop}}(\text{C-H})]$. $^1\text{H-NMR}$: (400 MHz, CDCl_3 solution, Me_4Si , 298 K) δ : 8.89 [2H, br, *ortho-H*_{4-Acpy}], 8.16 [4H, br, *ortho-H*_{Bz}], 7.79 [2H, br, *meta-H*_{4-Acpy}], 7.51 [2H, br, *para-H*_{Bz}], 7.40 [4H, br, *meta-H*_{Bz}], 2.65 [3H, s, CH_3] ppm. (UV-Vis: (MeOH , $6.5 \times 10^{-8} \text{ M}$) $\lambda_{\text{max}} = 201 \text{ nm}$; 222 nm; 272 nm.

4.5 Synthesis of of the compound $[\text{Cd}(\mu\text{-Bz})_2(4\text{-Acpy})_2]_2$ (4)

A MeOH solution (10 mL) of HBz (91.3 mg, 0.748 mmol) with 4-AcPy (186 mg, 1.54 mmol) was added dropwise to a MeOH solution (6 mL) of Cd(OAc)₂·2H₂O (101 mg, 0.377 mmol) and stirred for 18 h at r.t. Then, the solution was stirred under reflux conditions for 13 h. The resulting yellowish solution was concentrated until half of the volume and kept on fridge. After 15 h suitable yellow crystals were obtained. Crystals were filtered and washed with 10 mL of cold MeOH.

Yield: 126 mg (57%). Anal. Calc. for C₅₆H₄₈N₄O₁₂Cd₂ (1193.78 g mol⁻¹): C, 56.34; H, 4.05; N, 4.69. Found: C, 56.07; H, 3.94; N, 4.48%. ATR-FTIR (wavenumber, cm⁻¹): 3073(w), 3043(w), 3000(w) [$\nu(\text{CH})_{\text{ar}}$], 2981(w) [$\nu(\text{CH})_{\text{al}}$], 1695(m) [$\nu(\text{C}=\text{O})_{4\text{-AcPy}}$], 1595(m), 1548(m) [$\nu_{\text{as}}(\text{COO})$], 1533(m) [$\nu(\text{C}=\text{C})$, $\nu(\text{C}=\text{N})_{\text{ar}}$], 1493(w), 1392(s) [$\nu_{\text{s}}(\text{COO})$], 1362(s) [$\delta(\text{C}=\text{C})$, $\delta(\text{C}=\text{N})_{\text{ar}}$], 1014(m) [$\delta_{\text{ip}}(\text{C}-\text{H})$], 727(s), 715(s), 681(m) [$\delta_{\text{oop}}(\text{C}-\text{H})$]. ¹H-NMR: (400 MHz, CDCl₃ solution, Me₄Si, 298 K) δ : 8.90 [2H, br, *ortho*-H_{4-AcPy}], 7.97 [2H, d, ³J = 7.6 Hz, *ortho*-H_{Bz}], 7.69 [2H, d, ³J = 4.7 Hz *meta*-H_{4-AcPy}], 7.31 [1H, t, ³J = 7.3 Hz, *para*-H_{Bz}], 7.16 [2H, t, ³J = 7.5 Hz, *meta*-H_{Bz}], 2.57 [3H, s, CH₃] ppm. (UV-Vis: (MeOH, 4.2×10⁻⁶ M) λ_{max} = 202 nm; 222 nm; 277 nm.

4.6 X-ray crystallography

Colorless (**1-3**) and yellow (**4**) prism-like specimens were used for the X-ray crystallographic analysis. The X-ray intensity data were measured on a D8 Venture system equipped with a multilayer mono-chromate and a Mo microfocus ($\lambda = 0.71073$ Å). For **1-4**, the frames were integrated with the Bruker SAINT Software package using a narrow-frame algorithm. For **1**, the integration of the data using a monoclinic unit cell yielded a total of 35296 reflections to a maximum θ angle of 27.11° (0.78 Å resolution), of which 5564 were independent (average redundancy 6.344, completeness = 99.8%, $R_{\text{int}} = 8.42\%$, $R_{\text{sig}} = 5.00\%$) and 4248 (76.35%) were greater than $2\sigma(|F|^2)$. The calculated minimum and maximum transmission coefficients (based on crystal size) are 0.6464

and 0.7455. For **2**, the integration of the data using an orthorhombic unit cell yielded a total of 42047 reflections to a maximum θ angle of 38.60° (0.57 Å resolution), of which 8656 were independent (average redundancy 4.858, completeness = 99.7%, $R_{\text{int}} = 6.88\%$, $R_{\text{sig}} = 6.10\%$) and 5632 (65.06%) were greater than $2\sigma(|F|^2)$. The calculated minimum and maximum transmission coefficients (based on crystal size) are 0.5894 and 0.7476. For **3**, the integration of the data using a monoclinic unit cell yielded a total of 187379 reflections to a maximum θ angle of 28.38° (0.75 Å resolution), of which 13991 were independent (average redundancy 13.393, completeness = 99.0%, $R_{\text{int}} = 9.68\%$, $R_{\text{sig}} = 4.30\%$) and 9146 (65.37%) were greater than $2\sigma(|F|^2)$. The calculated minimum and maximum transmission coefficients (based on crystal size) are 0.5421 and 0.7457. For **4**, the integration of the data using a tetragonal unit cell yielded a total of 77802 reflections to a maximum θ angle of 30.06° (0.71 Å resolution), of which 7209 were independent (average redundancy 10.792, completeness = 99.5%, $R_{\text{int}} = 4.63\%$, $R_{\text{sig}} = 2.54\%$) and 6808 (94.44%) were greater than $2\sigma(|F|^2)$. The calculated minimum and maximum transmission coefficients (based on crystal size) are 0.3241 and 0.7460.

The structures were solved and refined using the Bruker SHELXTL Software, package and refined using SHELX (version-2018/3) [39]. For **1**, the final anisotropic full-matrix least-squares refinement on $|F|^2$ with 343 variables converged at $R_1 = 4.16\%$, for the observed data and $wR_2 = 8.52\%$ for all data. For **2**, the final anisotropic full-matrix least-squares refinement on $|F|^2$ with 219 variables converged at $R_1 = 4.82\%$, for the observed data and $wR_2 = 10.63\%$ for all data. For **3**, the final anisotropic full-matrix least-squares refinement on $|F|^2$ with 762 variables converged at $R_1 = 4.92\%$, for the observed data and $wR_2 = 14.78\%$ for all data. For **4**, the final anisotropic full-matrix least-squares refinement on $|F|^2$ with 337 variables converged at $R_1 = 2.66\%$, for the

observed data and $wR_2 = 5.86\%$ for all data. For **1-4**, the final cell constants and volume, are based upon the refinement of the XYZ-centroids of reflections above $20 \sigma(I)$. Data were corrected for absorption effects using the multi-scan method (SADABS). Crystal data and relevant details of structure refinement for compounds **1-4**, are reported in Table 6.

Table 6. Crystallographic data for **1-4**.

	1	2	3	4
Empirical formula	C ₂₈ H ₂₀ O ₈ Zn ₂	C ₁₄ H ₁₆ O ₇ Cd	C ₄₂ H ₃₄ N ₂ O ₁₀ Zn ₂	C ₅₆ H ₄₈ N ₄ O ₁₂ Cd ₂
Formula weight	615.18	408.67	857.45	1193.78
T (K)	100(2)	100(2)	100(2)	100(2)
Wavelength (Å)	0.71073	0.71073	0.71073	0.71073
System, space group	Monoclinic, P2 ₁ /c	Orthorhombic, Pbca	Monoclinic, C2/c	Tetragonal, P4 ₁ 2 ₁ 2
<i>Unit cell dimensions</i>				
<i>a</i> (Å)	10.8064(4)	9.6838(6)	17.307(3)	13.3285(5)
<i>b</i> (Å)	12.6391(4)	10.2466(6)	24.801(4)	13.3285(5)
<i>c</i> (Å)	18.8322(8)	30.956(2)	27.504(5)	27.8077(11)
α (°)	90	90	90	90
β (°)	100.670(2)	90	107.284	90
γ (°)	90	90	90	90
<i>V</i> (Å ³)	2527.69(16)	3071.6(3)	11273(3)	4940.0(4)
<i>Z</i>	4	8	12	4
<i>D</i> _{calc} (mg/m ³)	1.617	1.767	1.516	1.605
μ (mm ⁻¹)	1.949	1.453	1.340	0.931
<i>F</i> (0 0 0)	1248	1632	5280	2416
Crystal size (mm)	0.109x0.104x0.062	0.161x0.145x0.106	0.248x0.220x0.192	0.208x0.112x0.078
<i>hkl</i> ranges	-13 ≤ <i>h</i> ≤ 13 -16 ≤ <i>k</i> ≤ 16 -24 ≤ <i>l</i> ≤ 24	-14 ≤ <i>h</i> ≤ 16 -17 ≤ <i>k</i> ≤ 17 -54 ≤ <i>l</i> ≤ 53	-23 ≤ <i>h</i> ≤ 22 -33 ≤ <i>k</i> ≤ 33 -36 ≤ <i>l</i> ≤ 36	-18 ≤ <i>h</i> ≤ 18 -18 ≤ <i>k</i> ≤ 18 -39 ≤ <i>l</i> ≤ 37
2 θ range (°)	2.505 to 27.109	2.481 to 38.596	2.259 to 28.384	2.282 to 30.057
Reflections collected/unique/[<i>R</i> _{int}]	35296/5564/[<i>R</i> _{int} =0.0842]	42047/8656/[<i>R</i> _{int} =0.0688]	187379/13991/[<i>R</i> _{int} =0.0968]	77802/7209/[<i>R</i> _{int} =0.0463]
Completeness to θ	99.9%	99.9%	99.3%	99.4%
Absorption correction	Semi-empirical from equivalents	Semi-empirical from equivalents	Semi-empirical from equivalents	Semi-empirical from equivalents
Max. and min. transmission	0.7455 and 0.6464	0.7476 and 0.5894	0.7457 and 0.5421	0.7460 and 0.3241
Refinement method	Full-matrix least-squares on <i>F</i> ²	Full-matrix least-squares on <i>F</i> ²	Full-matrix least-squares on <i>F</i> ²	Full-matrix least-squares on <i>F</i> ²
Data/restraints/parameters	5564 / 0 / 343	8656 / 6 / 219	13991 / 19 / 762	7209 / 2 / 337
Goodness of fit on <i>F</i> ²	1.057	1.084	1.073	1.114
Final <i>R</i> indices [<i>I</i> > 2 σ (<i>I</i>)]	<i>R</i> ₁ = 0.0416, <i>wR</i> ₂ = 0.0779	<i>R</i> ₁ = 0.0482, <i>wR</i> ₂ = 0.0826	<i>R</i> ₁ = 0.0492, <i>wR</i> ₂ = 0.1100	<i>R</i> ₁ = 0.0266, <i>wR</i> ₂ = 0.0539
<i>R</i> indices (all data)	<i>R</i> ₁ = 0.0670, <i>wR</i> ₂ = 0.0852	<i>R</i> ₁ = 0.0954, <i>wR</i> ₂ = 0.1063	<i>R</i> ₁ = 0.0919, <i>wR</i> ₂ = 0.1478	<i>R</i> ₁ = 0.0322, <i>wR</i> ₂ = 0.0586

Extinction coefficient	n/a	0.00115(11)	n/a	0.0042(2)
Largest diff. peak and hole (e.Å ⁻³)	0.731 and -0.642	2.525 and -1.783	0.994 and -1.477	0.591 and -0.861

Molecular graphics were generated using Mercury 4.1.2 software [40] with POV-Ray package [41]. Color codes for all molecular graphics: Grey (C), white (H), red (O), light blue (N), blue (Zn), yellow (Cd). Crystal structures and molecular geometry are available in .cif format.

Conflicts of interest

There are no conflicts to declare.

Acknowledgements

This work was financed by CB615921 project, the Spanish National Plan of Research MAT2015-65756R, and 2017SGR1687 project from the Generalitat de Catalunya. The authors also acknowledge “Fundació La Caixa” for CB616406 endowment. F. S. acknowledges the PIF pre-doctoral fellowship from the Universitat Autònoma de Barcelona.

Appendix A. Supplementary data

CCDC-1972796-1972799 contains the supplementary crystallographic data for **1-4**. These data can be obtained free of charge *via* <http://www.ccdc.cam.ac.uk/conts/retrieving.html>, or from the Cambridge Crystallographic Data Centre, 12 Union Road, Cambridge CB2 1EZ, UK; fax: (+44) 1223-336-033; or e-mail: deposit@ccdc.cam.ac.uk.

References

- [1] L. Asgharnejad, A. Abbasi, M. Najafi and J. Janczak, *J. Solid State Chem.* 277 (2019) 187–194.
- [2] S.I. Noro, R. Ochi, Y. Inubushi, K. Kubo and T. Nakamura, *Microporous Mesoporous Mater.* 216 (2015) 92–96.

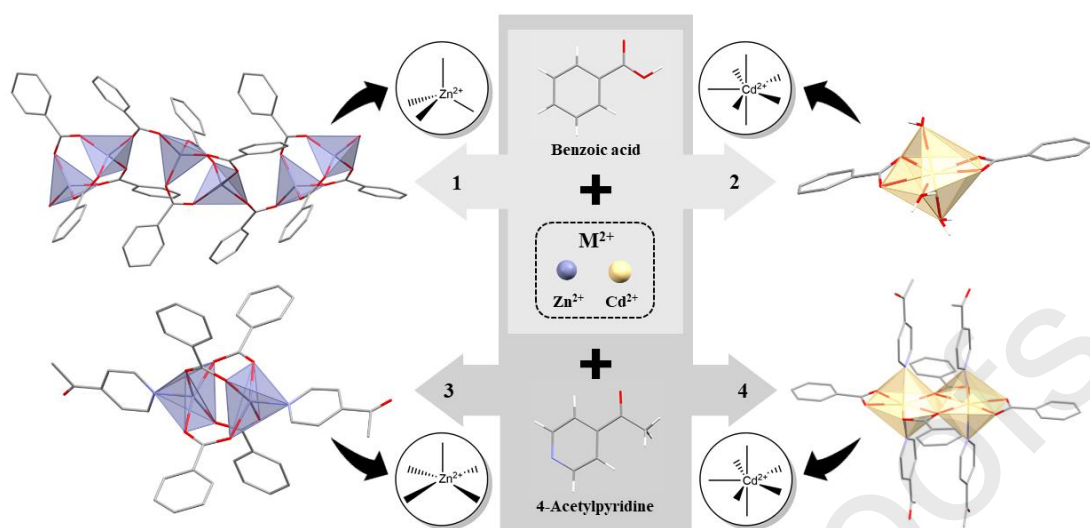
- [3] S.El-din, H. Etaiw and H. Marie, *Sensors Actuators, B Chem.* 290 (2019) 631–639.
- [4] J.M. Pan, Y.B. Ma, J. Shen, B. Liu, H. Liu, S.W. Jin and D.Q. Wang, *J. Coord. Chem.* 71 (2018) 2465–2486.
- [5] T.R. Cook, Y.R. Zheng and P.J. Stang, *Chem. Rev.* 113 (2013) 734–777.
- [6] G.R. Desiraju, *Acc. Chem. Res.* 35 (2002) 565-573.
- [7] E. Cimen, I. Gumus and H. Arslan, *J. Mol. Struct.* 1166 (2018) 397–406.
- [8] a) G.L. Clark, H. Kao, *J. Am. Chem. Soc.* (1948) 2151-2154.
b) G.A. Guseinov, F.N. Musaev, B.T. Usubaliev, I.R. Amiraslanov, Kh.S. Mamedov, *Koordinatsionnaia Khimiia* 10 (1984) 117
c) Yixun Zhang, A.W.Maverick, F.R.Fronczek CCDC 222164: Experimental Crystal Structure Determination, 2004
d) B.R. Bijini, S. Prasanna, M. Deepa, C.M.K. Nair, K.R. Babu, *Spectrochimica Acta, Part A: Molecular and Biomolecular Spectroscopy*, 97 (2012) 1002.
- [9] a) B. Başaran, E. Avşar, *Turk. J. Chem.*, 23 (1999) 243–247.
b) P. Anastas, N. Eghbali, *Chem. Soc. Rev.* 39 (2010) 301-312.
- [10] a) J.Q. Lin, C. Xiong, J.H. Xin, M. Li, W.H. Guo, F. Liu, X.L. Tong and Y.C. Ge, *J. Mol. Struct.* 1166 (2018) 1–6.
b) A. Morsali and M.Y. Masoomi, *Coord. Chem. Rev.* 253 (2009) 1882–1905.
- [11] H. Kwak, S.H. Lee, S.H. Kim, Y.M. Lee, B.K. Park, E.Y. Lee, Y.J. Lee, C. Kim, S.J. Kim and Y. Kim, *Polyhedron* 27 (2008) 3484–3492.
- [12] P. Lemoine, B. Viossat, N.H. Dung, A. Tomas, G. Morgant, F.T. Greenaway and J.R.J. Sorenson, *J. Inorg. Biochem.* 98 (2004) 1734–1749.
- [13] a) Y. Wang, L. Wang, X. Zhou, Y. Li, J. Li, *J. Mol. Struct.* 1173 (2018) 612-619.
b) J.-G. Zhang, W.-J. Gong, Y.-S. Guan, H.X. Li, D.J. Young and J.-P. Lang, *Cryst. Growth Des.* 18 (2018) 6172-6184.
- [14] K. Bania, N. Barooah and J.B. Baruah, *Polyhedron* 26 (2007) 2612–2620.
- [15] D. Dey, S. Roy, R.N. Dutta Purkayastha, R. Pallepogu and P. McArdle, *J. Mol. Struct.* 1053 (2013) 127–133.
- [16] A. Morsali and M.Y. Masoomi, *Coord. Chem. Rev.* 253 (2009) 1882–1905.
- [17] M. Guerrero, S. Vázquez, J.A. Ayllón, T. Calvet, M. Font-Bardia and J. Pons, *ChemistrySelect* 2 (2017) 632–639.
- [18] M. Guerrero, R. Pou, L. Bayés-García, M. Font-Bardia, J. Sort, J. Pons and J.A.

- Ayllón, *Inorg. Chem. Commun.* 96 (2018) 34–38.
- [19] F. Sánchez-Férez, R. Pou, L. Bayés-García, M. Font-Bardia, J. Pons and J.A. Ayllón, *Inorg. Chim. Acta* 500 (2020) 119218.
- [20] D. Ejarque, F. Sánchez-Férez, J.A. Ayllón, T. Calvet, M. Font-Bardia and J. Pons, *Cryst. Growth Des.* 20 (2020) 383-400.
- [21] A. Thirumurugan, M.B. Avinash, C.N.R. Rao, *J. Chem. Soc., Dalton Trans.* 60 (2006) 221–228.
- [22] D.H. Williams, I. Fleming, *Spectroscopic Methods in Organic Chemistry*, McGrawHill, London, UK, 1995.
- [23] J.Soldevila-Sanmartín, M. Sanchez-Sala, T. Calvet, M. Font-Bardia, J.A. Ayllón, J. Pons, *J. Mol. Struct.*, 1171 (2018) 808-814.
- [24] L. Yang, D.R. Powell and R.P. Houser, *Dalton Trans.* (2007) 955-964.
- [25] W. Clegg, D.R. Harbron, C.D. Homan, P.A. Hunt, I.R. Little and B.P. Straughan, *Inorg. Chim. Acta* 186 (1991) 51-60.
- [26] M. Nishio, *CrystEngComm* 6 (2004) 130-158.
- [27] X. Xue, Q. Wang, F. Mai, X. Liang, Y. Huang, J. Li, Y. Zhou, D. Yang and Z. Ma, *Molecules* 23 (2018) 1735.
- [28] W.J. Chu, H. Yong, Y.T. Fan and H.W. Hou, *Synth. React. Inorganic, Met. Nano-Metal Chem.* 40 (2010) 662-668.
- [29] R. Hoffmann, B.F. Beier, E.L. Muetterties and A.R. Rossi, *Inorg. Chem.* 16 (1977) 511-522.
- [30] K.H. Chung, E. Hong, Y. Do and C.H. Moon, *J. Chem. Soc., Dalton Trans.* (1996) 3363-3369.
- [31] T. Steiner, *Ange. Chem. Int., Ed.* 41 (2008) 48-76.
- [32] a) A.W. Addison and T.N. Rao, *J. Chem. Soc., Dalton Trans.* 1 (1984) 1349-1356.
b) E.L. Muetterties and L.J. Guggenberger, *J. Chem. Soc.* 96 (1974) 1748-1756.
- [33] a) A. Karkamar, R.J. Sarma and J.B. Baruah, *Inorg. Chem. Commun.* 9 (2006) 1169-1172.
b) K.H. Chung, E. Hong, Y. Do and C.H. Moon, *J. Chem. Soc., Dalton Trans.* (1996) 3363-3369.

- [34] a) J.E. Huheey, E.A. Keiter, R.L. Keiter, *Inorganic Chemistry. Principles of Structure and Reactivity*, 4th ed.; HarperCollins College Publishers: New York, USA, 1993.
- b) Sutton, D. *Electronic Spectra of Transition Metal Complexes*; McGraw-Hill: London, UK, 1975.
- [35] S. Tarasi, A. Azhdari Tehrani, A. Morsali, P. Retailleau, *New J. Chem.* 42 (2018) 14772–14778.
- [36] M.E. Sommer, M. Elgeti, P.W. Hildebrand, M. Szczepek, K.P. Hofmann, P. Scheerer, Elsevier Inc, Amsterdam, Netherlands, 2015.
- [37] R.F. Chen, *Anal. Lett.* 1 (1967) 35–42.
- [38] a) C. Würth, M. Grabolle, J. Pauli, M. Spieles, U. Resch-Genger, *Nat. Protoc.* 8 (2013) 1535–1550.
- b) G.M. Hale, M.R. Querry, *Appl. Opt.* 12 (1973) 555.
- [39] R.-P. Ye, X. Zhang, J.-Q. Zhai, Y.-Y. Qin, L. Zhang, Y.-G. Yao, J. Zhang, *CrystEngComm* 17 (2015) 9155–9166.
- [40] G.M. Sheldrick, *Acta Crystallogr. A.* 64 (2008) 112-122.
- [41] a) C.F. Macrae, P.R. Edgington, P. McCabe, E. Pidcock, G.P. Shields, R. Taylor, M. Towler and J. van de Streek, *J. Appl. Crystallogr.* 30 (2006) 453-457.
- b) C.F. Macrae, I.J. Bruno, J.A. Chisholm, P.R. Edgington, P. McCabe, E. Pidcock, L. Rodriguez-Monge, R. Taylor, J. van de Streek and P.A. Wood, *J. Appl. Crystallogr.* 41 (2008) 466-470.
- [42] Persistence of Vision Pty. Ltd. *Persistence of Vision (TM) Raytracer*; Persistence of Vision Pty. Ltd.: Williamstown, Australia, 2004; Available online: <http://www.povray.org/>

Highlights

- Reaction of metal oxides with HBz leads to polymer $[\text{Zn}(\mu\text{-Bz})_2]_n$ and monomer $[\text{Cd}(\text{Bz})_2(\text{H}_2\text{O})_3]$
- The incorporation of 4-Acpy yields $[\text{Zn}(\mu\text{-Bz})_2(4\text{-Acpy})]_2$ and $[\text{Cd}(\mu\text{-Bz})_2(4\text{-Acpy})_2]_2$
- The 4-Acpy sets square-pyramidal (Zn) or pentagonal-bipyramidal geometry (Cd)
- The molecular and supramolecular structures are discussed, obtaining 2D and 3D nets
- The UV-Vis and fluorescence spectra are recorded and their quantum yield calculated



CRedit author statement

Laura Moreno-Gómez: investigation, Writting – Original Draft, Visualization

Francisco Sánchez-Férez: investigation, Writting – Original Draft, Visualization

Teresa Calvet: Validation, Resources, Writing – Review & Editing, Funding acquisition

Mercè Font-Bardia: Validation, Formal analysis, Data Curation

Josefina Pons: Conceptualization, Validation, Resources, Writing – Review & Editing, Supervision, Project administration, Funding acquisition

Journal Pre-proofs